Finite Element Modeling of Thermal Fatigue and Damage of Solder Joints in a Ceramic Ball Grid Array Package

BOR ZEN HONG

IBM Microelectronics Division, Hopewell Junction, NY 12533

A nonlinear finite element model is presented for analyzing the cyclic and thermal fatigue loading and for viscoplastic damage characterization of the lead-tin (Pb-Sn) solder joints in a ceramic ball grid array (CBGA) surface mount package. An approach using a $\Delta \epsilon_{eq}^{in}$-modified Coffin-Manson equation is proposed to estimate the fatigue life of the solder joints. The $\Delta \epsilon_{eq}^{in}$ represents a *saturated* equivalent inelastic strain range as determined by the finite element model. The present study shows that the predictied fatigue life and the associated damage mechanism of the solder joint agree reasonably well with the test data for the 18, 25, and 32 mm CBGA packages run at a cyclic temperature load of 0°C/100°C with a frequency of 1.5 cycles per hour. Analysis also shows that a preferred failure site is expected to occur in and around the Pb37-Sn63 solder attachment of the solder joint. A time-dependent (creep induced) damage mechanism is found to be more pronounced than the time-independent (plastic deformation) mechanism.

Key words: Ceramic ball grid array (CBGA), finite element, ratcheting, solder joint, thermal fatigue, viscoplastic

INTRODUCTION

In recent years, the ascendance of the electronic packaging engineering to a pivotal position has promoted a unifying trend to the high density surface mount interconnection technology. Surface mounting in electronic systems using solder bonding method allows semiconductor chip or chip carrier to be attached directly to a printed circuit board (PCB) or card. Advanced ceramic ball grid array (CBGA) surface mount package has recently become an attractive alternative to the fine-pitched quad flat pack (QFP) package for high density interconnections in the microelectronics industry.[1,2] The CBGA package was developed to serve as a mechanical and electrical connection for attaching the ceramic substrate to the PCB or card as shown in Fig. 1. As in many surface mount electronic systems, the subject of thermal fatigue problem of solder joints is central to much of the reliability of CBGA packages.

Thermal fatigue of solder joint is essentially a low cycle fatigue. It is a thermally induced viscoplastic deformation process caused by the expansional mismatch in a package subjected to cyclic changes in temperature. The direct measurement of thermally induced viscoplastic deformation of the solder joint is not a straightforward task. This is mainly due to the structural complications and miniaturization of the solder joint as well as due to the available measuring instrumentations and experimental methods of acceptable accuracy. Therefore, the use of appropriate modeling methods and analytical tools is recommended to provide the solutions for the thermal fatigue and damage problems of electronic packages.[3–9]

Most prior thermal fatigue analyses of solder joints have relied on the so-called global thermal mismatch method.[3,4] This approach uses a distance from the neutral plane (DNP) concept to calculate the shear strain purely due to the global mismatch of thermal expansions between the two components adjacent to the solder joint. The calculated shear strain is assumed to be experienced by the solder joint and is treated as a fully time-independent plastic strain necessary for using the Coffin-Manson equation and

(Received December 18, 1996; accepted February 28, 1997)

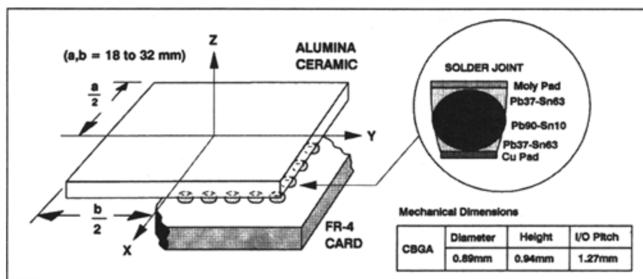

Fig. 1. Ceramic ball grid array (CBGA) package.

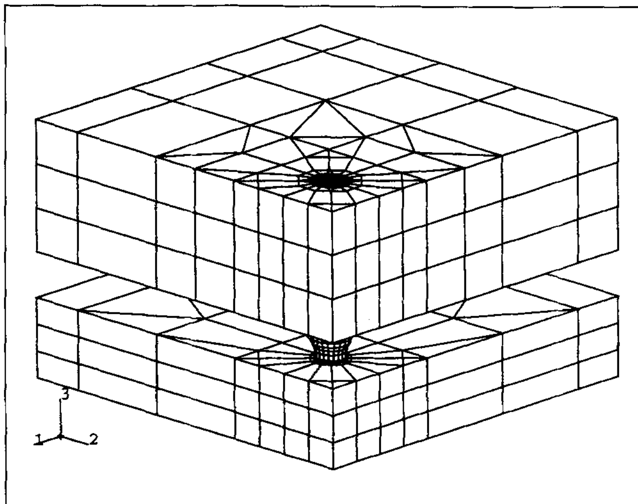

a

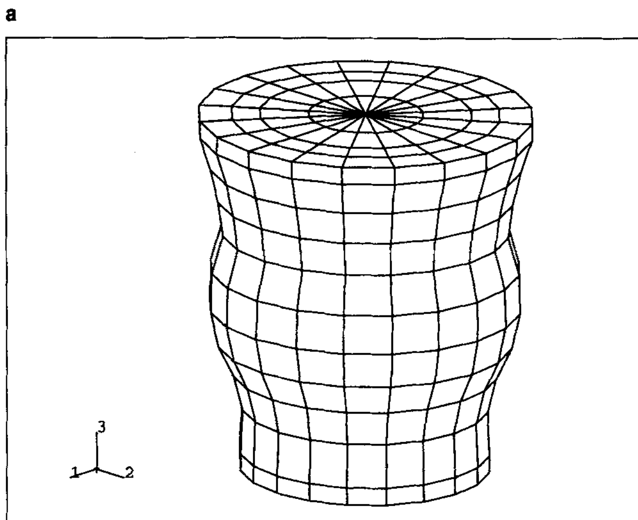

b

Fig. 2. Finite element model of the CBGA package: (a) mesh of a quarter of CBGA package, and (b) enlarged mesh of CBGA solder joint.

its modified versions to predict the thermal fatigue life of the solder joint in the electronic package. This approach has the merit of simplicity; however, it may lead to inaccurate estimations.

The errors are largely due to the neglect of several important factors that affect the thermal deformation and fatigue behavior of the solder joint. They are, namely,

- The multi-axial rather than the pure shear loading and response,
- Local thermal mismatch between the solder joint and the connected components,
- Time and temperature dependent properties of solder joint,
- Their induced cyclic creep (ratcheting) behavior, and
- Creep-fatigue interactions.

To address this concern, the use of nonlinear finite element approach is necessary and has been successfully practiced for various surface mount packages.[5–9]

In this paper, an engineering approach using a nonlinear finite element model and a deformation-based life analysis method will be presented. The goal is to study the thermally induced viscoplastic deformation damage and the life prediction of solder joints in a CBGA surface mount package under a cyclic temperature load.

FINITE ELEMENT MODELING OF A CBGA PACKAGE

Model Description

In this study, a three-dimensional finite element model was created to represent a CBGA surface mount package. This package has a 32 mm square alumina ceramic substrate connected to a 156 × 107 mm FR-4 card with a number of Pb-Sn solder joints. These solder joints have a dimension of 0.89 mm diameter and 0.94 mm height, and are placed on an I/O pitch of 1.27 mm on the substrate. The solder joint has a Pb90-Sn10 solder ball embraced by the eutectic Pb37-Sn63 solder paste at both ends. (See Fig. 1) A 25 μm thick molybdenum pad is used as the ceramic connection to the solder joint and the copper pad is for the card connection. Because of symmetry, only one quarter of the surface mount package was modeled. The finite element mesh was created using the I-DEAS® Master Series Program.[10]

For the sake of computing efficiency, only one solder joint located in the edge with the maximum DNP was considered in the model. The global-local mesh, as shown in Fig. 2, has two different types of solid finite elements (six-node wedge and eight-node brick) with a total of 1743 elements and 1548 nodes in the model. For comparison, two other CBGA packages with the size of 18 and 25 mm, respectively, were also included in this study.

Low Cycle Thermal Fatigue Loads

In analysis, a uniform constant temperature distribution was assumed and prescribed across the whole package. A low cycle thermal fatigue load of 0°C/100°C was applied to the modeled package. Figure 3 gives the detailed profile of cyclic thermal fatigue load used for numerically studying the thermal stresses and viscoplastic strains in the modeled CBGA package. A total of three cycles with a 10 min hold time, a temperature ramp rate of 10°C/min, and a frequency of 1.5 cycles per hour (cph) was applied in the finite element simulation. The room temperature (25°C) is treated as the initially stress-free temperature.

Constitutive Properties of Materials

In this work, metallic and alloy materials are assumed to be elastic-plastic (copper and molybdenum) and elastic-viscoplastic (Pb37-Sn63 and Pb90-Sn10), respectively. The nonmetallic materials (alumina and FR-4) are linearly elastic. A constitutive theory of thermoviscoplasticity based on classical creep and plasticity concept was used in modeling thermally induced deformation behavior of the Pb-Sn solder joints.[5] In the theory, the total strain is assumed to be the sum of the elastic, plastic, creep, and thermal strains. The Garofalo hyperbolic sine law was applied to model the creep behavior, while the Prandtl-Reuss equation was used for rate-independent plastic deformation. Details of the constitutive theory are described in Hong and Burrell.[5] The material properties of the surface mount package components are listed in Table I.[5,6,8,11] It is obvious that the temperature dependence is significant for the modulus, Poisson ratio, yield strength, and thermal expansion coefficient of Pb-Sn alloys. Figures 4 and 5 give the temperature dependent stress-strain data for the Pb90-Sn10 and Pb37-Sn63 solder alloys, respectively.[11]

Numerical Simulation

In simulation, the modeled problems were solved by using a nonlinear finite element program, ABAQUS®.[12] Numerical simulations were carried out in an IBM RISC/6000 computer system. The computing times for simulating three cycles of thermal fatigue load were typically 8 to 16 h for the three studied cases (18, 25, and 32 mm CBGA packages). A preferred maximum time integration step of 10 s was determined for ensuring the solution accuracy.

Distributions of Stress and Strain

The results of peak thermal stress and strain are found to occur in the Pb37-Sn63 solder paste of the corner solder joint. The corner solder joint is located at the highest DNP location of the CBGA package, as shown in Fig. 2. The finite elements of the Pb37-Sn63 solder paste in the corner solder joint are extracted from the whole model, as shown in Fig. 6a. They will be used for describing the maximum inelastic response of the edge CBGA solder joint. The element numbered 559 of the Pb37-Sn63 solder paste is located at the upper corner near to the interface between the solder paste and the ceramic molybdenum pad. For convenience, the following notations are

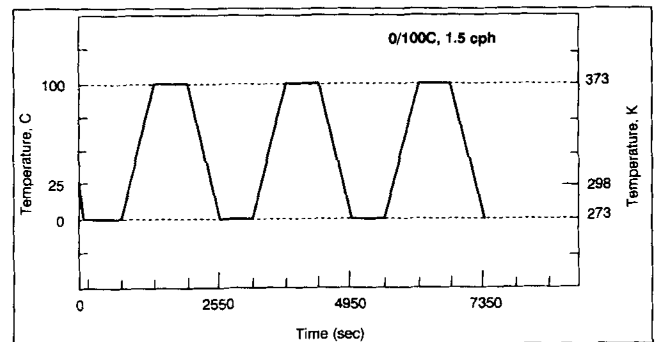

Fig. 3. Temperature cycle for the modeled CBGA package.

Table I. Material Properties of CBGA Package[5,6,8,11]

Material	Dimension (mm)	Temp. (K)	Elastic Modulus (MPa)	Poisson Ratio	Yield Strength (MPa)	CTE (ppm/K)	Thermal Conductivity (W/m-K)	Specific Heat (J/kg-K)	Density (kg/m)^3
Alumina Ceramic Substrate	2.9 thick	298	300000	0.23	elastic	6.7	21	765	3970
Molybdenum Ceramic Pad	0.89 Dia. 0.025 thick	298	320000	0.28	552.0	5.0	138	251	10240
Pb90-Sn10 Solder Ball	0.89 Dia.	273 323 373	16342[11] 9612 6000	0.40 0.40 0.40	14.3[11] 12.6 5.8	27.8 28.2 28.6	36	148	10500
Pb37-Sn63 Solder Paste	0.75 Dia. | 0.89 Dia.	273 323 373	26447[11] 12521 6909	0.360 0.365 0.378	36.4[11] 15.2 9.6	25.2 26.1 27.3	51	150	8470
Copper Card Pad	0.89 Dia. 0.025 thick	298	117000	0.34	69.0	16.7	389	385	8942
FR-4 Card	1.83 thick	298	18200	0.25	elastic	15.0	13	879	1938

Creep Law: 1. Pb90-Sn10: $\dot{\epsilon}^{cr} = 275.42 (\sinh 0.52\sigma)^{0.47} \exp(-60000/RT)$.[5]
2. Pb37-Sn63: $\dot{\epsilon}^{cr} = 12423.2 (\sinh 0.125938\ \sigma)^{1.88882} \exp(-61417/RT)$.[8]

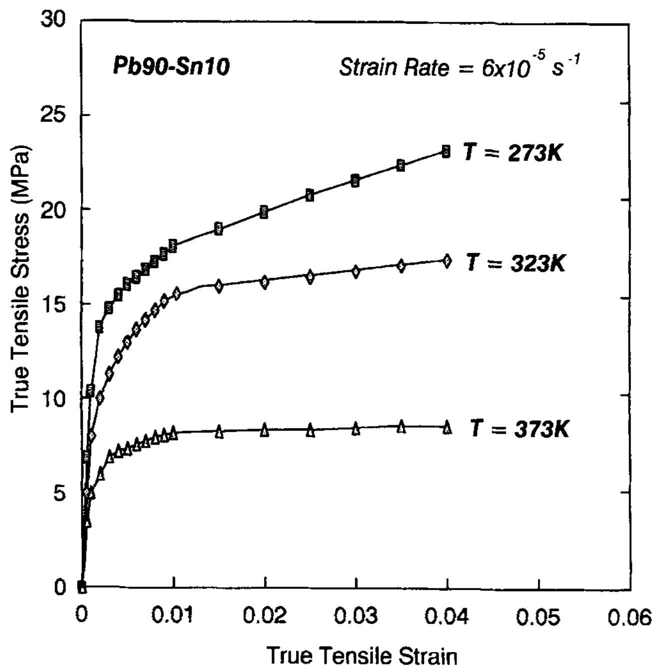

Fig. 4. Temperature-dependent stress-strain data for Pb90-Sn10 alloy.[11]

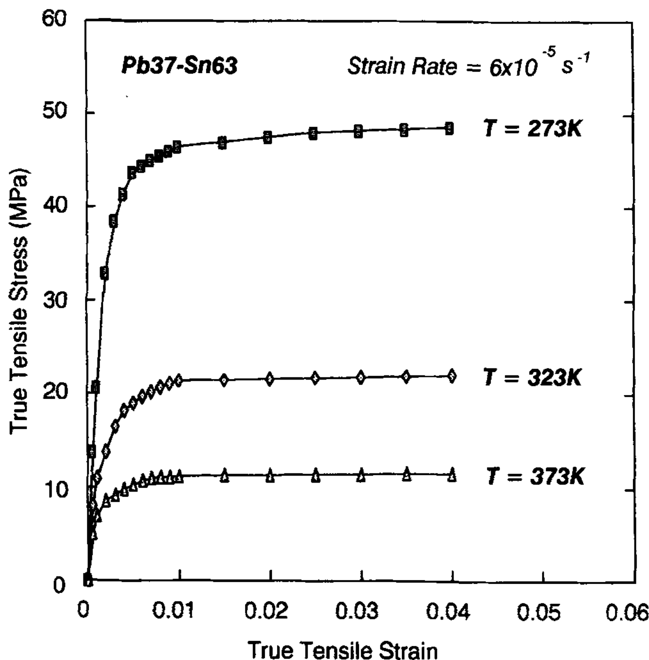

Fig. 5. Temperature-dependent stress-strain data for Pb37-Sn63 alloy.[11]

used to report the analysis results. The σ^{v}_{eq} is the von Mises stress (MISES), ϵ^{cr}_{eq} is the equivalent creep strain (CEEQ), and ϵ^{pl}_{eq} is the equivalent plastic strain (PEEQ), respectively.

Figures 6b–6d give the respective contour plots of peak σ^{v}_{eq}, ϵ^{cr}_{eq}, and ϵ^{pl}_{eq} for the corner solder joint in a 32 mm CBGA package under a total of three cycles of 0°C/100°C load. The results for the solder joint at the end of the third cycle are presented. The analysis shows that the peak values of stress and strain occur in and around the interface between the Pb37-Sn63 paste and the Pb90-Sn10 ball, and that between the Pb37-Sn63 paste and the moly pad, respectively. It is obvious that the cracking failure may initiate at one of these two interfaces. Crack propagation and complete failure is expected to occur within the Pb37-Sn63 paste. This is consistent with the preferential failure sites of the solder joint as shown in the test results of the CBGA packages.[13,14]

Ratcheting (Cyclic Creep) Behavior

Ratcheting is a phenomenon that occurs when the creep strain accumulates in a material system subjected to a fully reversal, cyclic constant load or stress. *Ratcheting* is also called *cyclic creep* or *incremental collapse* in literature. The shear responses of ratcheting in the selected element (559) of the Pb37-Sn63 paste are compared in Fig. 7 for 18, 25, and 32 mm CBGA packages, respectively. Here the conventional sign (sense) notation is used for the shear response of the solder joint in the modeled package. The stress-strain hysteresis loops will ratchet (travel) in the direction from right to left (i.e., in the direction from the corner to the center of the package) for the Pb37-Sn63 solder paste. This will create a relative motion in the Pb37-Sn63 paste between the moly pad and the Pb90-Sn10 ball, from which it becomes the driving force for initiating cracking failure in this region. For clear representation, only the responses at the first and the third cycle are presented.

Figure 8 shows the histories of the maximum ϵ^{cr}_{eq} and ϵ^{pl}_{eq} of the Pb37-Sn63 paste corresponding to Fig. 7. They are all increasing functions of time (or cycle). The step-type results present in both time-dependent and time-independent responses. The ϵ^{pl}_{eq} grows in the ramp temperature duration and stays as plateau in the hold-time (dwell). On the contrary, the ϵ^{cr}_{eq} develops and accumulates more in the hold-time duration. It is shown that the creep response is approximately one order of magnitude higher than the plastic response in the Pb37-Sn63 paste. As a summary, the Pb37-Sn63 paste has a more pronounced time-dependent (creep) damage mechanism than that of the time-independent (plastic) deformation. This may be due to the fact that the eutectic Pb-Sn solder alloys have a low resistance to creep deformation.[15] It can be also seen that the larger package size has the effect of increasing inelastic strain response in the Pb37-Sn63 paste of the solder joint.

THERMAL FATIGUE LIFE ANALYSIS

Concept of Saturated Inelastic Strain Range $\left(\Delta \epsilon^{in}_{eq}\right)$

Assessing the brief results just presented, and other similar results,[5,6,16,17] it is assumed that the ratcheting response of the solder joint may reach a *saturated state* after a certain number of thermal cycles. To verify this assumption, another numerical test was exercised to study the ratcheting response of the Pb37-Sn63 solder paste in the solder joint of a 32

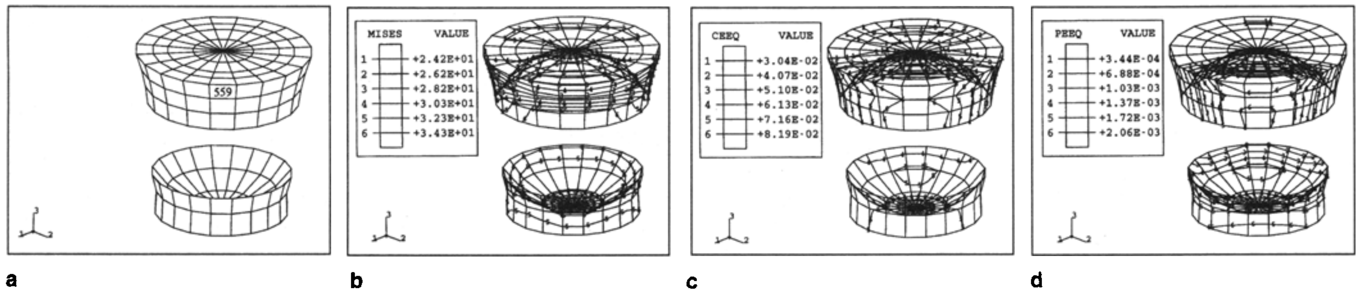

Fig. 6. FEA results of Pb37-Sn63 solder paste in the highest-DNP solder joint of a 32 mm CBGA package under a cyclic load of 0/100°C with a frequency of 1.5 cph. Response of stress and strain at the end of the third cycle are plotted: (a) the extracted FE mesh of Pb37-Sn63 paste, (b) contour of Mises stress, (c) contour of equivalent creep strain, CEEQ, and (d) contour of equivalent plastic strain, PEEQ.

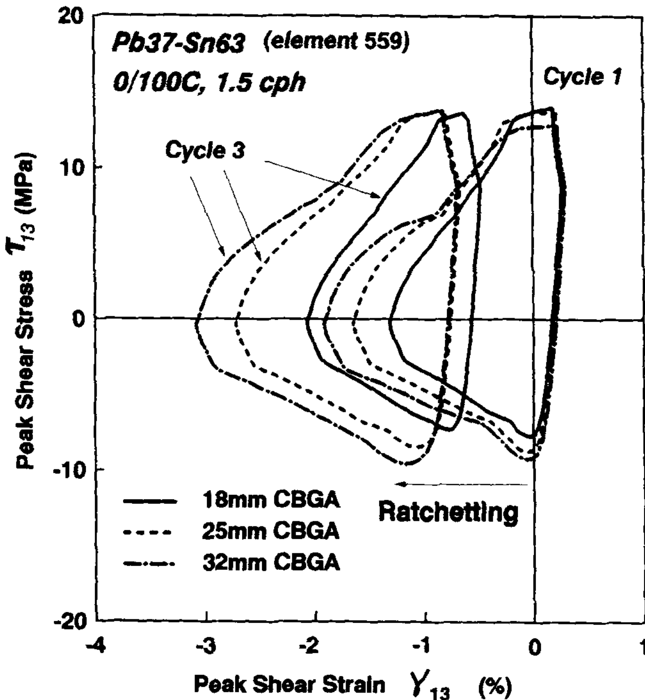

Fig. 7. Effect of module size on ratcheting response of Pb37-Sn63 paste in the CBGA solder joint.

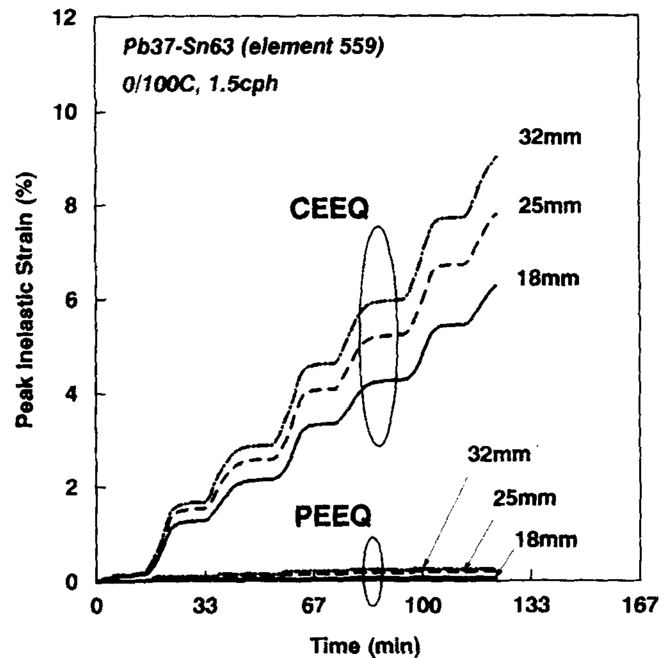

Fig. 8. Effect of module size on inelastic strain response corresponds to Fig. 7. CEEQ: equivalent creep strain; PEEQ: equivalent plastic strain. CEEQ is 10x of PEEQ.

mm CBGA package under a 20 cycles of 0°C/100°C load. The result of shear ratcheting is shown in Fig. 9a. It is seen that the cyclic creep at a decreasing rate (denser hysteresis loop at high strain) continues at substantially constant stress throughout the running period. However, the corresponding strain amplitude stays approximately constant of each hysteresis loop, by comparing the magnitude of the first cycle vs that of the twentieth cycle. It should be noted that the number of temperature cycles, N_t, is different from the number of cycles to thermal fatigue failure, N_f, as used in the Coffin-Manson law for life analysis. The former (N_t) is the number of cycles prescribed in the model as a loading condition; the result of accumulated inelastic strain response of the solder joint is found to be an increasing function of N_t. On the other hand, the latter (N_f) is a decreasing function of the inelastic strain range in the Coffin-Manson law.

The peak values of the thermally induced inelastic strains, as occurred in the element 559 of the Pb37-Sn63 paste of the solder joint at the end of each cycle, are compared in Table II for various packages. It is clear that from the results for each package the accumulated magnitude and rate of ϵ_{eq}^{cr} are significantly higher than that of ϵ_{eq}^{pl}. For example, the ratio of ϵ_{eq}^{cr} to ϵ_{eq}^{pl} is as high as 70–110 in three cycles for 18 mm package when compared to the larger packages. The 25 mm package is 30–40, and the 32 mm package is 20–40, respectively. These accumulated ϵ_{eq}^{cr} and ϵ_{eq}^{pl} can also be used for characterizing the thermally induced damage mechanisms and identifying the dominant mechanism.

To estimate the cycles to thermal fatigue failure, N_f, of the solder joint, it is necessary to compute the peak values of the total equivalent inelastic strain, ϵ_{eq}^{in}, and the total equivalent inelastic strain range, $\Delta\epsilon_{eq}^{in}$, respectively, of the Pb37-Sn63 solder paste (the preferred failure site of the solder joint). Here, the ϵ_{eq}^{in} is defined as the sum of ϵ_{eq}^{cr} and ϵ_{eq}^{pl}. The $\Delta\epsilon_{eq}^{in}$ accounts for the difference between those ϵ_{eq}^{in} at each two consecutive cycles for each Pb37-Sn63 paste in the solder joint for various CBGA packages. By carefully examining these $\Delta\epsilon_{eq}^{in}$, we find they have a *saturated*

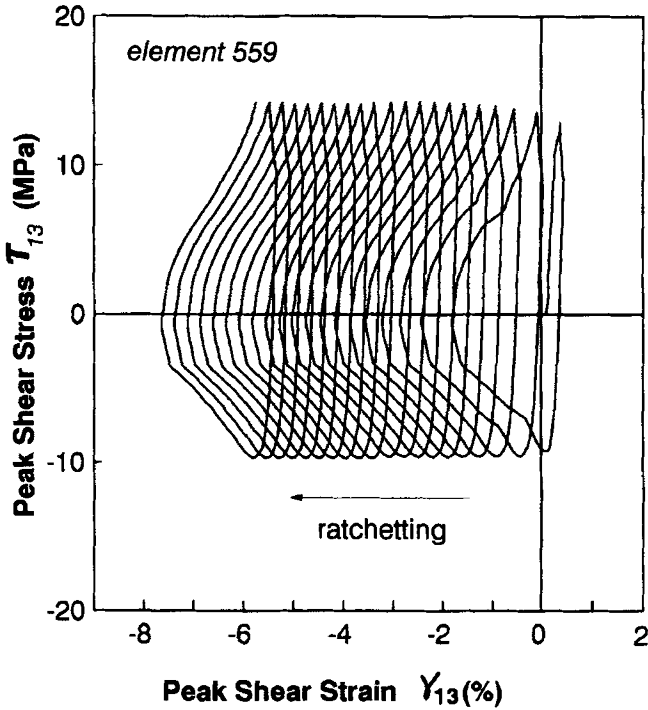

a

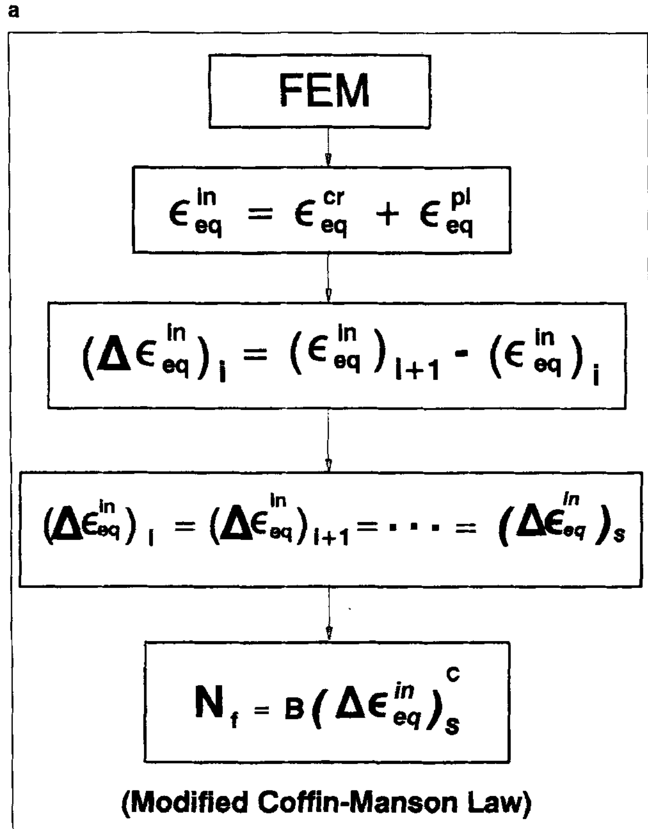

b

Fig. 9. Saturated $\Delta\epsilon^{in}_{eq}$ concept and thermal fatigue life prediction: (a) ratcheting response of Pb37-Sn63 solder paste in the largest DNP solder joint of a 32 mm CBGA package under 20 cycles of 0/100°C load with f = 1.5 cph, and (b) life analysis flow.

value for the solder joint in each modeled package during the three simulated temperature cycles. Note

Table II. Maximum Inelastic Response of CBGA Solder Joints Temperature Load: 0/100C, Frequency = 1.5 cph

N_t	CEEQ	PEEQ	IEEQ	ΔIEEQ
18 mm CBGA Package (Pb37-Sn63, Element 559)				
1	2.011E-02	2.896E-04	2.040E-02	2.040E-02
2	4.048E-02	4.482E-04	4.093E-02	2.053E-02
3	6.103E-02	5.475E-04	6.158E-02	2.065E-02
25 mm CGBA Package (Pb37-Sn63, Element 559)				
1	2.526E-02	7.506E-04	2.601E-02	2.601E-02
2	5.078E-02	1.536E-03	5.232E-02	2.631E-02
3	7.692E-02	1.920E-03	7.884E-02	2.652E-02
32 mm CBGA Package (Pb37-Sn63, Element 559)				
1	2.865E-02	1.310E-03	2.996E-02	2.996E-02
2	5.854E-02	2.042E-03	6.058E-02	3.062E-02
3	8.931E-02	2.356E-03	9.167E-02	3.109E-02

that the *saturated* $\Delta\epsilon^{in}_{eq}$ includes the combined effects of ratcheting and plasticity, and is a function of material and the applied load.

Thermal Fatigue Life Prediction

In this study, we assume that such *saturated* $\Delta\epsilon^{in}_{eq}$ will remain constant for the Pb37-Sn63 solder paste until the final failure occurs in the solder joint (See Table II and Fig. 9a). Based on this hypothesis, the saturated $\Delta\epsilon^{in}_{eq}$ as determined from the finite element model, can be used as a compatible measure of merit for replacing the purely time-independent plastic strain range, $\Delta\epsilon_p$, in the conventional Coffin-Manson law. Therefore, a ϵ^{in}_{eq}-modified Coffin-Manson equation is formulated as

$$\left(N_f \nu^{k-1}\right)^{\alpha} \Delta\epsilon^{in}_{eq} = 0 \qquad (1)$$

where N_f is the number of cycles to failure, ν is the cyclic frequency, and α, θ, and k are material constants, respectively. These material constants were found to be temperature dependent for the eutectic Pb-Sn alloys as reported by Solomon.[18] From his study, the influence of frequency is mainly controlled by the value of k. Given the scattered data of N_f vs ν, the best fitting curves were obtained when k = 1 for the isothermal fatigue test run at –50, 35, and 150°C, respectively, when 2×10^{-4} Hz < ν < 0.3 Hz (See Fig. 12 and Fig. 13 in Solomon).[18] Here, for k = 1, it implies that there is no frequency effect on the fatigue life of solder material when the frequency is in a specific range. In the present study, the cyclic frequency is 1.5 cph (= 4.2×10^{-4} Hz), which is within the range as mentioned above. Therefore, by letting k = 1, Eq. (1) can be rewritten as

$$N_f = B\left(\Delta\epsilon^{in}_{eq}\right)^C \qquad (2)$$

for calculating the thermal fatigue life of the solder joint. The material constants, α = 0.51, θ = 1.41, B =

1.2928, and C = –1.96, for the eutectic Pb40-Sn60 solder alloy are obtained from the average values of those in the isothermal fatigue tests run at –50, 35, and 125°C.[18] In this work, brief procedures of the deformation-based life analysis method are summarized in Fig. 9b. Included are

- Finite element modeling for calculating temperature dependent viscoplastic deformation of solder joint, and
- A concept of the saturated inelastic strain range in conjunction with a modified Coffin-Manson law for life prediction.

In principle, the knowledge of temperature dependent viscoplastic material properties and constants of solder alloys is necessary for this approach. This can be obtained from the isothermal monotonic and fatigue test data at various temperatures that cover the range of temperatures for thermal cycling in simulation.

To determine the usability of the present deformation-based life analysis method, the present calculated values of thermal fatigue life, N_{50}, for the solder joint are compared with those obtained by a Monte Carlo simulation and actual tests for various CBGA packages.[14] Numerical results, test data, and comparison are presented in Table III. From the results, it is observed that the inclusion of the present thermal fatigue life analysis method shows a favorable accuracy of solution within 10% for the selected 18, 25, and 32 mm CBGA packages.

CONCLUSIONS

In this paper, a nonlinear finite element model was used to study the thermal fatigue and damage behavior of the solder joints in a CBGA package under a cyclic temperature load of 0°C/100°C.

Analysis shows that the preferential failure will initiate at the interface between the Pb37-Sn63 paste and the ceramic moly pad through the competitive damage mechanisms of creep and plasticity. Complete failure in the Pb37-Sn63 solder paste of the solder joint occurs as expected. This confirms the test results.[13,14]

There are two competitive damage mechanisms, caused by creep and plasticity, respectively, in the CBGA solder joint. The time-dependent response of creep is more pronounced in the Pb37-Sn63 solder paste than that of the time-independent plastic response.

An engineering approach of $\Delta \epsilon_{eq}^{in}$-modified Coffin-Manson equation was proposed to estimate the thermal fatigue life of the CBGA solder joint. The predicted results agree reasonably well with the test data.[14] These results for the thermal fatigue life prediction of CBGA solder joints should serve as a reference for future comparison since the thermal fatigue is a time-dependent statistical process.

Table III. Prediction of Thermal Fatigue Life of CBGA Solder Joint

Pb37-Sn63 in Solder Joint (0/100C, 1.5 cph)	$\Delta \epsilon_{eq}^{in}$ [a] FEM	N_{50} FEM[b] Prediction	N_{50} Monte[c] Carlo Simulation	N_{50} Test[c] Data
18 mm CBGA	0.02053	2625	2300	2900
25 mm CBGA	0.02628	1618	1854	1649
32 mm CBGA	0.03056	1204	1263	1231

[a]The $\Delta \epsilon_{eq}^{in}$ is the average value obtained from the ΔIEEQ in Table II and is assumed as the "saturated" value.
[b]Present study: fatigue life is calculated using Eq. (2).
[c]From G. Phelan and S. Wang (1993).[14]

ACKNOWLEDGMENTS

The author is grateful to Harish D. Merchant, Gould Electronics, who invited me to write this paper and made comprehensive comments during the preparation of the manuscript. Technical discussions with Lew Goldmann, Peter Brofman, and Lloyd Burrell are acknowledged. For management support, my special thanks go to Peter Ulanmo and Hal Lasky.

REFERENCES

1. T. Caulfield, J.A. Benenati and J. Acocella, *Proc. Int. Conf. and Exh. of MultiChip Modules,* (ISHM, 1993), p. 320.
2. J.U. Knickerbocker and M.S. Cole, *Adv. Packaging* Jan./Feb., 20 (1995).
3. K.J. Lodge and D.J. Pedder, *Proc. 40th ECTC,* (New York: IEEE, 1990), p. 470.
4. W. Englemaier, *Soldering & Surface Mount Techn.* 10, 18 (1992).
5. B. Hong and L.G. Burrell, *IEEE Trans.* CPMT-A, 18 (3), 585 (1995).
6. B. Hong and L.G. Burrell, *Proc. of I-THERM V Conf.,* (New York: ASME/IEEE, 1996), p. 158.
7. A.R. Syed, *Trans. of ASME, J. Electron. Packaging* 117, 116 (1995).
8. T.Y. Pan, *Trans. of ASME, J. Electron. Packaging* 113, 8 (1991).
9. B. Ozmat, *Proc. 40th ECTC,* (New York: IEEE, 1990), p. 959.
10. I-DEAS® Master Series, (Milford, OH: Structural Dynamics Research Corp., 1996).
11. M.S. Cole, T. Caulfleld, D.R. Banks, M.M. Winton, A.P. Walsh and S.G. Gonya, *Proc. Materials Dev. in Microelectronic Packaging Conf.,* Montreal, Quebec, Canada, (Metals Park, OH: ASM, 1991), p. 241.
12. ABAQUS® Version 5.5, (Providence, RI: Hibbit, Karlson and Sorensen, Inc., 1996).
13. M.D. Ries, D.R. Banks, D.P. Watson and H.G. Hoebener, *IBM J. Res. & Dev.* 37 (5), 597 (1993).
14. G. Phelan and S. Wang, *Proc. 43th ECTC,* (New York: IEEE, 1993), p. 858.
15. J.S. Huang, and R.M. Vargas, *Soldering & Surface Mount Techn.* (5), 38 (1990).
16. B. Hong, *Proc. 1996 IEPS Con.,* (IEPS, 1996), p. 256.
17. B. Hong, T. Yuan and L.G. Burrell, *ASME 1996 Int. Mech. Eng. Congress & Exposition,* Atlanta, GA, 1996.
18. H.D. Soloman, *IEEE Trans. CHMT*-9 (4), 423 (1986).